



THREE-DIMENSIONAL ATOMIC STRUCTURE OF NiO–ZrO₂(CUBIC) INTERFACES

E. C. DICKEY^{†1}, V. P. DRAVID¹, P. D. NELLIST^{‡2}, D. J. WALLIS^{§3} and S. J. PENNYCOOK²

¹Materials Science and Engineering Department, Northwestern University, Evanston, IL 60208, U.S.A.,
²Solid State Division, Oak Ridge National Laboratory, Oak Ridge, TN 37831, U.S.A. and ³Department of Physics (M/C), University of Illinois at Chicago, Chicago, IL 60607, U.S.A.

(Received 29 August 1996; accepted 8 July 1997)

Abstract—The three-dimensional atomic structure of low-energy NiO–ZrO₂(cubic) interfaces is determined through a combination of electron imaging and spectroscopy techniques. High resolution electron microscopy, and Z-contrast STEM imaging with simultaneous electron energy loss spectroscopy are employed as complementary techniques for elucidating the structural and chemical aspects of the interface and associated interfacial relaxation mechanisms. The planar interfaces show an atomically abrupt transition between the two phases which share a common oxygen plane at the boundary. Structural relaxations accommodating the lattice mismatch indicate that the boundary has relaxed to a low-energy configuration. The resulting interface structure is found to facilitate strong bonding across the boundary as is reflected in the fracture behavior of the composite system. © 1998 Acta Metallurgica Inc.

1. INTRODUCTION

Internal heterophase interfaces are pervasive in composite materials and often influence or even control bulk material properties. Establishing fundamental interface structure–property relationships is therefore essential for designing and tailoring interfaces in such multi-component material systems. By elucidating the interrelated constituents of interface structure (geometry, chemistry and electronic structure), one can begin to understand the influence of the interface on relevant bulk material properties, deducing atomic structure/property relationships. While interface science has been particularly successful in advancing our understanding of grain boundary atomic structure and its influence on material properties, our understanding of heterophase interfaces is relatively immature. Recent high resolution electron microscopy (HREM) studies have successfully revealed the atomic structure of various heterophase interfaces including metal–metal, metal–ceramic and metal–semiconductor types (see, for example, Refs [1–5]). Ionic heterophase interfaces, an important class of ceramic interfaces, have not, however, been as widely investigated on an atomic scale. Some notable exceptions include

the investigations of MgO–Al₂O₃ interfaces by Li *et al.* [6] and spinel–Al₂O₃ interfaces by Carter and Schmalzried [7], as well as others [8–10].

This paper is part of an ongoing research effort to explore the atomic structure of a number of oxide–oxide boundaries with the aim of establishing predictive structure–property relationships for such ionic heterophase interfaces. For this research we investigate pseudo-binary eutectics which have been directionally solidified. Directionally solidified eutectics (DSEs) are advantageous for interface studies for numerous reasons [11], but are particularly attractive because they are amenable to the three-dimensional characterization necessary to understand the complete structure of the boundary and its intimate connection to bonding, electrical transport, etc. Many DSE systems fulfill the requirements for three-dimensional analysis: they have planar interfaces and orientation relationships in which low-index zone axes are aligned in at least two directions. This paper explores the detailed atomic structure of low-energy NiO–ZrO₂(cubic) interfaces and the associated interfacial relaxation mechanisms. Some specific questions driving this research and related to interface atomic structure are:

- (1) How does the interface accommodate a transition in chemistry, projected point symmetry (3 m in NiO and 4 mm in ZrO₂), and oxygen coordination (tetrahedral in NiO and octahedral in ZrO₂)?
- (2) What interfacial relaxation mechanisms prevail in these highly ionic systems?

[†]Current address: Department of Chemical and Materials Engineering, University of Kentucky, Lexington, KY 40506-0046, U.S.A.

[‡]Current address: Cavendish Laboratory, Madingley Road, Cambridge CB3 0HE, U.K.

[§]Current address: Defence Research Agency, St. Andrews Road, Malvern, Worcestershire WR14 3PS, U.K.

(3) What implications does the interface structure have for bonding across the interface?

To answer these questions, we have employed a variety of electron imaging and spectroscopy techniques including HREM, Z-contrast scanning transition electron microscopy (STEM) imaging and electron energy loss spectroscopy (EELS). Traditionally, HREM has been the primary analytical technique in interfacial studies because of its ability to elucidate interface structure on an atomic scale [2, 12]. Another powerful approach, however, which has been developed in more recent years, is to combine Z-contrast STEM imaging with spatially-resolved electron energy loss spectroscopy (EELS) to obtain atomic-resolution chemical and structural information simultaneously [13, 14]. Both approaches have distinct advantages and disadvantages for determining interface structure, so we use them synergistically to gain maximum information about the NiO–ZrO₂ interface. From the experimental information we draw conclusions about the nature of the interface structure and its implications for bonding in ionic heterophase systems.

2. EXPERIMENTAL PROCEDURES

2.1. Sample preparation

NiO–ZrO₂(cubic) eutectics were directionally solidified at the Laboratoire de Chimie at the Université de Paris-Sud. Eutectic proportions of NiO and ZrO₂ powders along with a stabilizer additive (CaO or Y₂O₃) were isostatically pressed into cylindrical rods and sintered. The rods were then directionally solidified by the floating zone technique associated with a double ellipsoid image furnace [15]. The bulk samples contain several large grains having a lamellar microstructure (see Fig. 1). Each grain is essentially two interpenetrating single crystals which have well-defined crystallographic orientation relationships. The bulk samples are strongly textured with $[\bar{1}10]_{\text{NiO}} \parallel [010]_{\text{ZrO}_2} \parallel \text{growth direction}$; this texture aids in preparing specimens along particular crystallographic directions.

For transmission electron microscopy (TEM) sample preparation, sections were cut from the bulk specimens using a precision diamond saw and were thinned to approximately 10 μm using a tripod pol-

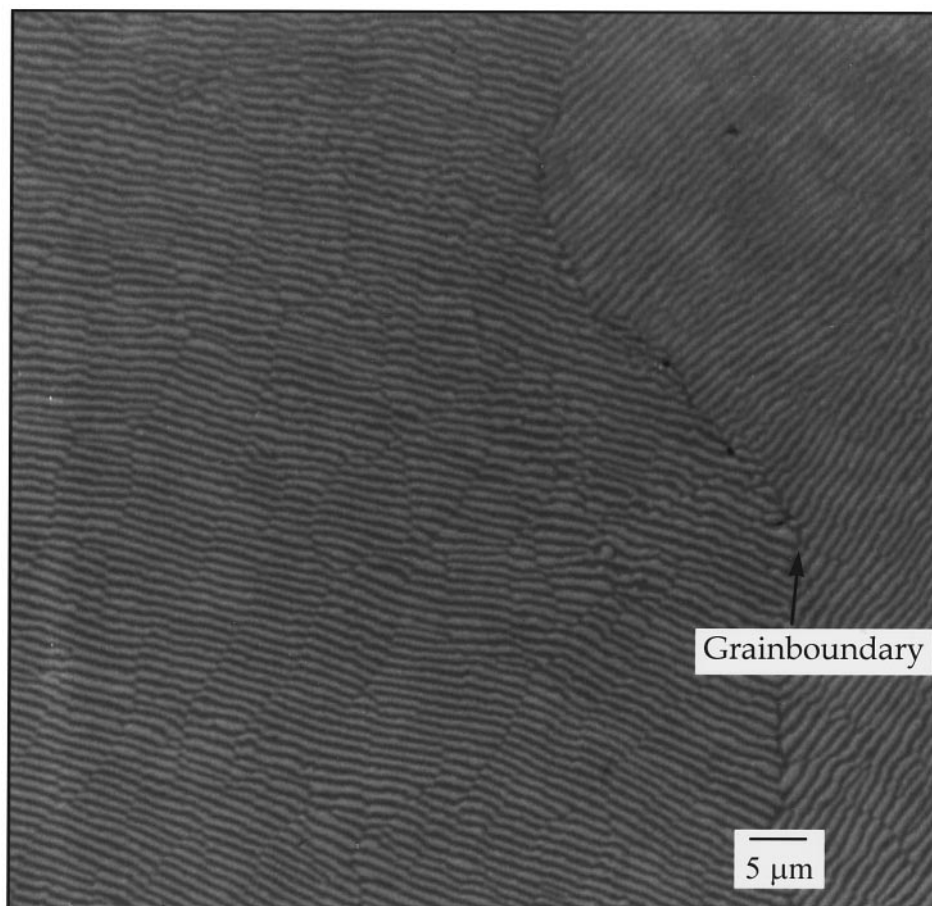


Fig. 1. Optical micrograph of the NiO–ZrO₂(cubic) DSE lamellar microstructure which gives rise to planar interfaces between the two phases.

isher and diamond lapping film. The samples were subsequently polished with colloidal silica and mounted onto slotted copper grids. Because of the differential thinning rates of the two phases, it was crucial that the samples be $\leq 10 \mu\text{m}$ before ion milling. The samples were milled to electron transparency in a Gatan Duo-Mill at liquid nitrogen temperatures using 1 mA of 5 keV Argon ions. To remove any amorphous surface layers, the foils were finally milled with 3 keV Ar ions and annealed for 1 hr at 500°C in oxygen.

2.2. HREM

HREM was employed to reveal the geometric aspects of the interface structure including the translation state of the two lattices, local atomic relaxations and the terminating planes constituting the interface. A through-focus-series of images of $[\bar{1}10]_{\text{NiO}}\parallel[010]_{\text{ZrO}_2}$ was taken using a Hitachi H9000, a 300 kV TEM with a point resolution of 0.18 nm. The relevant lattice spacings (ZrO₂ (200) at 0.256 nm and NiO (111) at 0.241 nm) were therefore easily resolved in the first pass band. The microscope parameters used in image simulations were: C_s (spherical aberration coefficient) = 1 mm, α (illumination convergence angle) = 1.5 mrad and ΔE (focal spread) = 10 nm.

Imaging the $[11\bar{2}]_{\text{NiO}}\parallel[001]_{\text{ZrO}_2}$ specimens posed a greater challenge because of the small 0.148 nm NiO (220) fringes running perpendicular to the boundary. Although the NiO (220) spacing could be imaged under large defocus conditions in the H9000, it was difficult to find conditions favorable for the transfer of NiO (220) at 0.148 nm, NiO (111) at 0.241 nm and ZrO₂ (200) at 0.256 nm. Even when such conditions were achieved, the gradient of the transfer function about these spacings was quite large, leading to delocalization of the image. To circumvent the problems associated with conventional HREM, the specimens were imaged in the JEOL JEM-ARM1250 at the Max-Planck Institut für Metallforschung in Stuttgart. Using the side entry pole piece at 1250 kV, this instrument has a $C_s = 2.8$ mm and a 0.12 nm theoretical point resolution which is sufficient to image the 0.148 nm NiO (220) fringes within the first pass band [16]. Negatives from both the JEOL ARM and the H9000 were digitized to eight bits using an Optronics P1000 microdensitometer, and the images were corrected for scan distortions.

2.3. Multislice simulations

In order to interpret the detailed interface atomic structure from HREM images, multislice simulations were carried out on a HP workstation using NUMIS[®] software developed at Northwestern University. The supercell models used in the image simulations were necessarily large, 1.023 nm ($[11\bar{2}]_{\text{NiO}}\parallel[001]_{\text{ZrO}_2}$) \times 2.068 nm ($[\bar{1}10]_{\text{NiO}}\parallel[010]_{\text{ZrO}_2}$) \times 7.215 nm (perpendicular to the interface), in order

to prevent aliasing and to account for lattice mismatch while including integral numbers of unit cells. For phase grating calculations, the supercells were sliced into less than 0.2 nm increments along the beam direction and the sampling was greater than 40 nm^{-1} .

2.4. Z-contrast imaging and maximum entropy refinement

The NiO–ZrO₂ interfaces were also imaged in the 300 kV VG Microscopes HB603U STEM ($C_s = 1$ mm) at Oak Ridge National Laboratory. A large-angle annular detector was used to produce a transversely incoherent image. Because relatively high-angle scattering is collected (inner radius of annular detector = 30 mrad), the Z-contrast image intensity scales with atomic number, yielding peaks of intensity at the cation sites [17, 18]. Under incoherent imaging conditions, the spatial resolution is limited by the probe size, in this case 0.13 nm. Consequently, the HB603 could successfully resolve all of the necessary spacings along $[\bar{1}10]_{\text{NiO}}\parallel[010]_{\text{ZrO}_2}$ and $[11\bar{2}]_{\text{NiO}}\parallel[001]_{\text{ZrO}_2}$.

To quantify atomic positions from the Z-contrast images, maximum entropy reconstruction was performed. Since the image is simply a convolution of the object function and the probe function, we can extract the probe function from the bulk lattice where the object function is known precisely. (The method for probe reconstruction is outlined in detail by Nellist and Pennycook [19].) Using the reconstructed probe function, we then reconstruct the object function in the defect area (in this case the NiO–ZrO₂ interface) by the maximum entropy image reconstruction technique developed by Gull and Skilling [20]. The resulting object function is used for quantitative analysis. We find that object functions derived from images recorded at a magnification of 10^7 times yield positional accuracies of 0.01 nm.

2.5. Electron energy loss spectroscopy (EELS)

To characterize the chemistry of the interfaces, EELS spectra were collected on a 100 kV HB501UX STEM. Under channeling conditions, individual atomic columns are excited, providing a near atomic-resolution spectrum for most core loss edges [13, 14].

Profiles of the Ni L_{2,3}, Zr M_{4,5} and O K-edges were collected parallel to the boundary plane. The Z-contrast image was used to position the probe accurately, and line profiles parallel to the boundary were acquired in steps of interplanar spacing (e.g. NiO(111) and ZrO₂ (200)). At each position four spectra were collected for 2.5 s each. Spectra at the beginning and end of a series were compared to ensure that no electron beam damage had occurred during the acquisition. Between each set of spectra, the probe was repositioned using the Z-contrast image to check or compensate for drift

during the collection. Only those spectra in which no detectable drift or beam damage occurred were used for analysis. The energy resolution of the parallel energy-loss spectrometer, as determined by the full-width half-maximum of the zero-loss peak, was 1.1 eV and the dispersion was 0.303 eV/channel over 385 channels. Each spectrum was corrected for the response function of the detector, and the background was fit to a power-law over a 50 eV window preceding the edge onset and subtracted from the spectrum.

EELS was also used to explore the changes in local oxygen coordination near the interface through changes in the oxygen K near-edge fine structure. The near-edge fine structure results from perturbations to the unoccupied electron states lying just above the Fermi level introduced by the surrounding atoms and reflects the local coordination, bonding and valence state of the atom undergoing excitation [21, 22]. Therefore, by collecting energy-loss spectra from individual planes parallel to the interface, the spatial extent of local changes in coordination and atomic structure can be determined.

3. RESULTS AND DISCUSSION

In this section we reveal the NiO–ZrO₂ interface structure as determined by HREM, Z-contrast and EELS experiments. The interface structure is a complex, multifaceted issue which can be described from a macroscopic level down to an atomic level. We address most of the characteristics of the interface structure which collectively lead to an atomic model of the boundary. First we define the interface on a macroscopic scale, describing its morphology and the relative crystallographic orientation relationships between the two phases. We then explore the chemistry of the interface to reveal the

possible presence of interdiffusion. By using a combination of techniques we determine the chemistry at an atomic scale, identifying the terminating planes of the two crystals at the interface. Finally we discuss the mechanisms by which the interface relaxes to a low-energy configuration; these include local atomic relaxations as well as rigid body translations of the two crystals. All of these aspects of the interface structure finally lead us to an atomic model of the boundary which is consistent with experimental results from all of the electron imaging and spectroscopy techniques.

3.1. Interface morphology and macroscopic degrees of freedom

On a macroscopic scale, the NiO–ZrO₂ interfaces are planar and have no porosity, impurities or reaction phases, allowing for intimate contact between the two phases at the interface (see Fig. 2). The predominant orientation relationship between the phases, which defines the five macroscopic degrees of freedom associated with the boundary, is [11]:

$$(111)_{\text{NiO}} \parallel (100)_{\text{ZrO}_2}$$

$$[\bar{1}10]_{\text{NiO}} \parallel [010]_{\text{ZrO}_2}$$

This orientation relationship provides the opportunity to image the edge-on interface from two orthogonal directions, revealing the three-dimensional structure (see Fig. 3). (The abbreviations OR I, OR II and OR III as outlined in Fig. 3 will be used to identify the orientation of the interface throughout the remainder of the paper.) Macroscopic curvature of the boundary is accommodated by atomic steps which have ledges with the above orientation relationship, indicating that this orientation relationship is indeed a low-energy configuration [11]. Figure 4 is a plan-view projection of the interface.



Fig. 2. HREM image of the planar NiO–ZrO₂ interfaces which are free from voids and impurity or reaction phases.

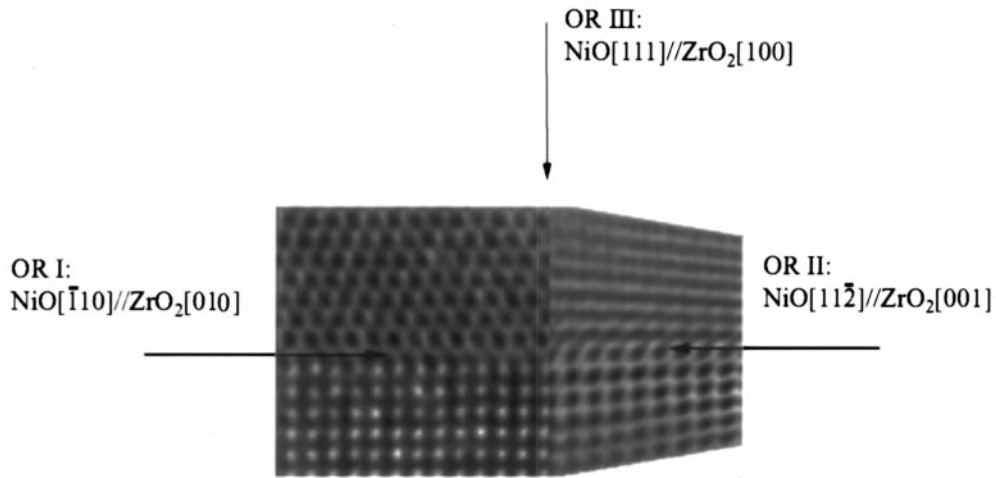


Fig. 3. Schematic of planar NiO–ZrO₂(cubic) interfaces. The edge-on interface can be viewed along two orthogonal directions (OR I and OR II), revealing the three-dimensional structure.

Note that there is a one-to-one correspondence between the ZrO₂ and NiO lattice as viewed from OR I; the lattice mismatch between NiO (111) as projected onto the interface plane and ZrO₂ (200) is only 0.4%. In the orthogonal direction (OR II), however, the lattice mismatch between NiO(110) and ZrO₂(020) is very large, over 14%. The relaxation mechanisms accommodating the lattice mismatch and reducing the interfacial energy are

expected to be quite different along these two orthogonal directions.

3.2. Interface chemistry

The chemistry of the interface was probed using EELS. Figure 5 is a profile of the Ni L_{2,3} edge taken in steps of interplanar spacing across the NiO–ZrO₂ interface. Similar profiles were taken of the Zr M_{4,5} and O K edges. To measure the chemi-

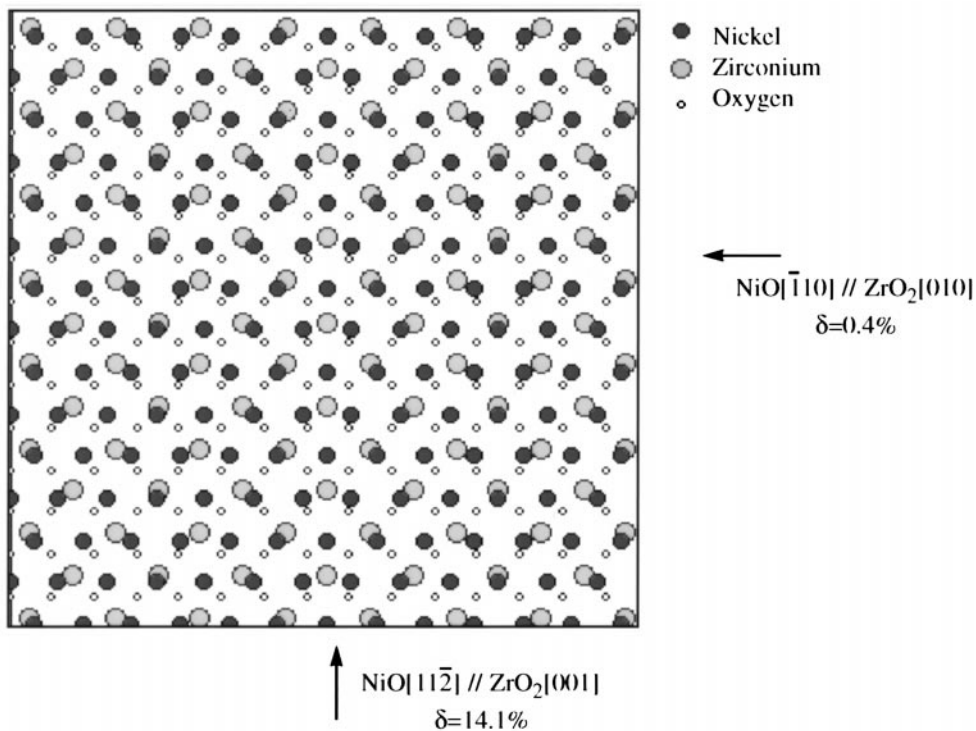


Fig. 4. Plan-view projection of the NiO–ZrO₂ interface. While the lattices are nearly perfectly commensurate along OR I, the lattices are incommensurate along OR II.

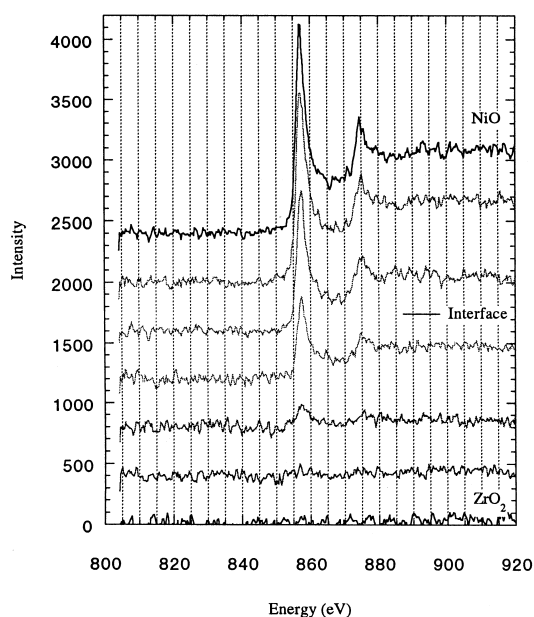


Fig. 5. Example of a Ni L_{2,3} EELS profile taken in steps of interplanar spacing across the NiO-ZrO₂ interface.

cal width of the boundary, the integrated intensity of a profile (from edge onset past the near-edge fine structure) was normalized to the integrated intensity of a bulk spectrum. The resulting chemical profiles are presented in Fig. 6 in which each data point results from the average of several profiles. The vertical error bars represent the first standard deviation of the normalized intensities and the horizontal error bars are the estimated positioning error of the probe.

Although the elemental profiles presented in Fig. 6 show a chemical width of about two atomic planes or about 0.3 nm, this profile is in fact consistent with an chemically abrupt interface. Two

factors lead to the apparent broadening of the chemical width. First, the inelastic scattering processes giving rise to the core-loss edges have an inherent object function size depending on the electronic transition energy. For K and L edges the full width half maximum of the object function can be on the order of an angstrom [23,24]. Secondly, some residual intensity in the interface planes may be attributed to an experimental probe having tails with finite intensities that can excite columns of atoms adjacent to the probe position. With an objective aperture size of 10 mrad in the VG HB501, the resulting probe would serve to smear a step function to a profile having a width (defined by the width between 75% and 25% intensity) of 0.15 nm. The apparent width of the elemental profile presented in Fig. 6 is therefore attributed to both the finite size of the object function and the tails of the experimental probe. Consequently, the chemical profile results are consistent with an atomically abrupt interface.

3.3. Common oxygen plane

Because the two crystals have an orientation relationship which results in a layered structure of anion and cation planes parallel to the interface, it has been hypothesized that the two phases maintain this anion-cation sequence across the boundary by sharing a common oxygen plane at the interface [25]. Such a model certainly makes sense from an electrostatic point of view and would facilitate a chemically abrupt transition between the two phases. We aim to confirm this structure because it has important implications for bonding at the interface.

Figure 7 is a Z-contrast STEM image of the NiO-ZrO₂ interface taken along OR I. Although the Z-contrast images are not sensitive to the oxy-

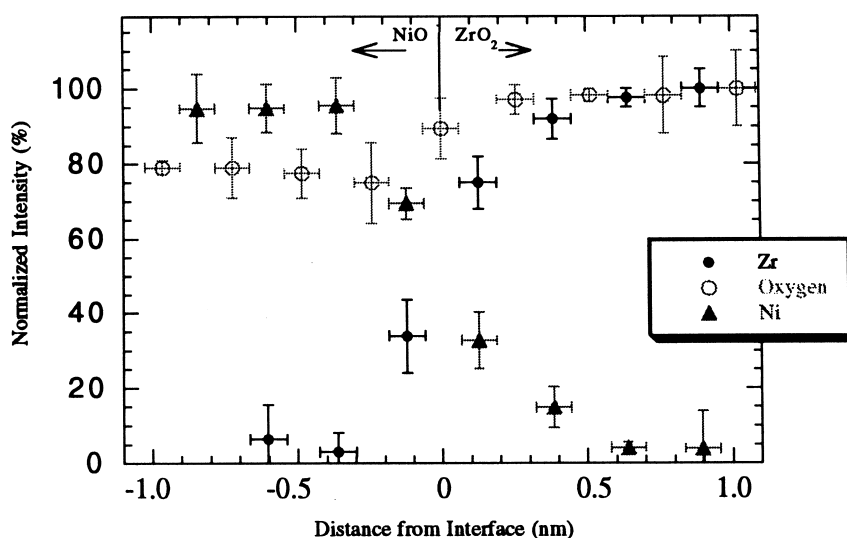


Fig. 6. Profiles of Ni, Zr and O normalized intensities across the NiO-ZrO₂ interface.

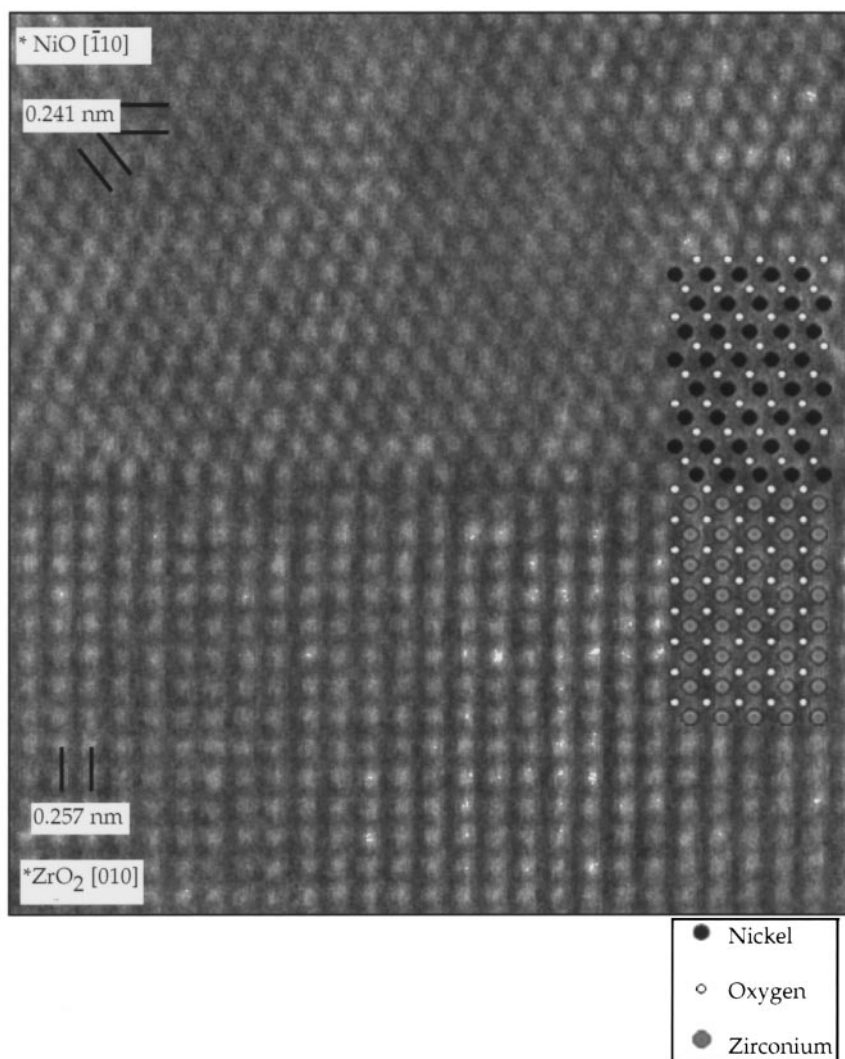


Fig. 7. Z-contrast image of NiO–ZrO₂ interface along OR I with interface model superimposed.

gen positions, they reveal an atomic spacing between the terminating Ni and Zr planes which is intermediate to that of the bulk NiO (111) and ZrO₂ (200) and sufficiently large to accommodate a common oxygen plane. While by itself Z-contrast does not confirm the common oxygen plane, EELS results presented above verify that oxygen is present between the last Ni and Zr planes (see Fig. 6). We see, in fact, that the common oxygen plane has a concentration of oxygen intermediate to those of bulk NiO and ZrO₂. The model of the interface containing the common oxygen plane projected along OR I is superimposed on the Z-contrast image in Fig. 7. Note the excellent agreement between the Z-contrast image and the cation sites in the model. The significance of this particular model will be discussed in more detail in Section 3.5.

The presence of a common oxygen plane between NiO and ZrO₂ is also confirmed by HREM. Two images from a through-focus series along OR I were used for analysis, one taken in the first large

pass band [Fig. 8(a)] and the other in the second pass band [Fig. 8(b)]. The interface model presented in Fig. 7 was used for multislice simulations. The sample thickness was determined to be 3.2 nm and the defoci –42 and –71 nm. The results of the multislice calculations are inset in the experimental images (Fig. 8) and identified by brackets. Note that the black contrast in Fig. 8(a) corresponds to the cation sites in both phases, whereas the white contrast in Fig. 8(b) corresponds to the cation sites. The excellent agreement between the simulated and experimental structures corroborates the interface structure presented in Fig. 7.

It is interesting to note that other oxide heterophase systems maintain similar orientation relationships resulting in homopolar surfaces at the interface; these include NiO–CaO [26], NiO–Y₂O₃ [27], Al₂O₃–ZrO₂(cubic) [28] and Fe₂O₃–Al₂O₃ [29]. From the results of the NiO–ZrO₂, we may infer that these other systems also share a common oxygen plane at the interface which leads

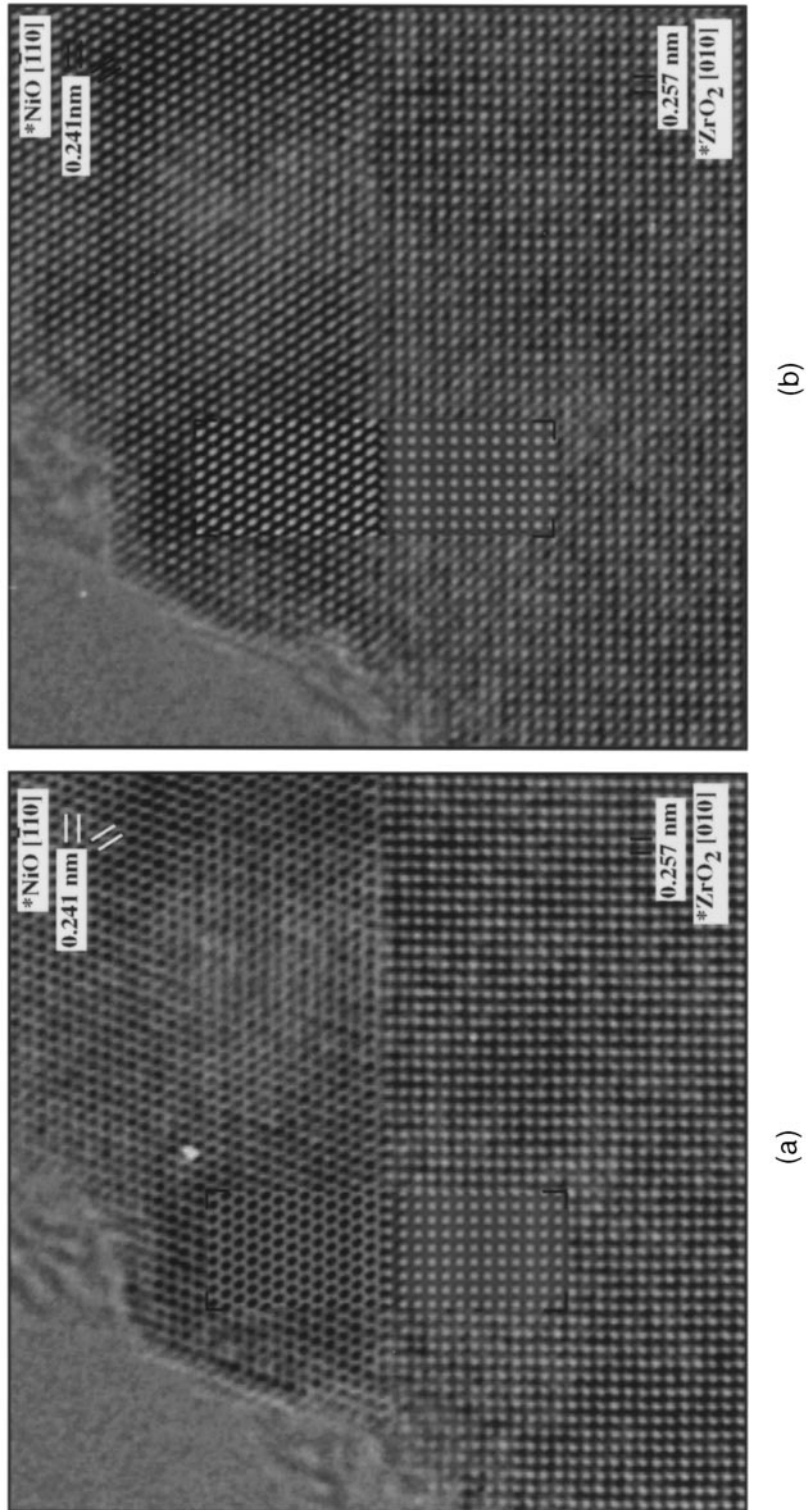


Fig. 8. HREM images of NiO–ZrO₂ along OR I: (a) $\Delta f = -42$ nm, (b) $\Delta f = -74$ nm. Results of multislice simulations are included in brackets.

to electrostatic bonding across the boundary. This trend suggests that low-energy orientation relationships in ionic materials are governed not only by lattice misfits, but also by the polarity of the planes constituting the interface.

3.4. Local atomic relaxation

Several mechanisms exist by which bicrystals can relax to lower their interfacial energy; these include rigid body translations (RBT) and local atomic relaxations. We will first address the issue of local relaxation since it offers evidence that the interface has indeed relaxed to a low-energy configuration and thus makes the discussion of RBT more relevant.

First consider the interface as projected along OR I. Since no misfit dislocations are observed over a length exceeding 22.5 nm (see Fig. 2), the room temperature 0.4% lattice mismatch must be completely accommodated by elastic strain in the two phases. Since the NiO is the more compliant material along that direction, it is presumed to assume the majority of the strain.

Even though the boundary appears completely coherent along OR I, one appreciates the true complexity of the interface when it is imaged along the orthogonal direction (OR II) where the lattice mismatch is very large, 14.1% between NiO (110) and ZrO₂ (200). Initial studies of this orientation were performed on the Hitachi H9000 at large values of defoci which would facilitate transfer of the 0.148 nm NiO (220) fringes (see Fig. 9). Although the image is delocalized at the interface and thus difficult to interpret, the bending of NiO (220) fringes near the boundary suggests that interface has relaxed to a low-energy configuration. To confirm this relaxation, the interface was imaged along OR II in the Stuttgart JEOL JEM-ARM1250 (see Fig. 10). In this case the image is much more localized at the interface, and the NiO (220) lattice fringes still bend within about 0.5 nm of the interface. Individual atomic columns in NiO become difficult to distinguish in the last two planes adjacent to the interface as a consequence of strain from misfit dislocations. The positions of the interfacial

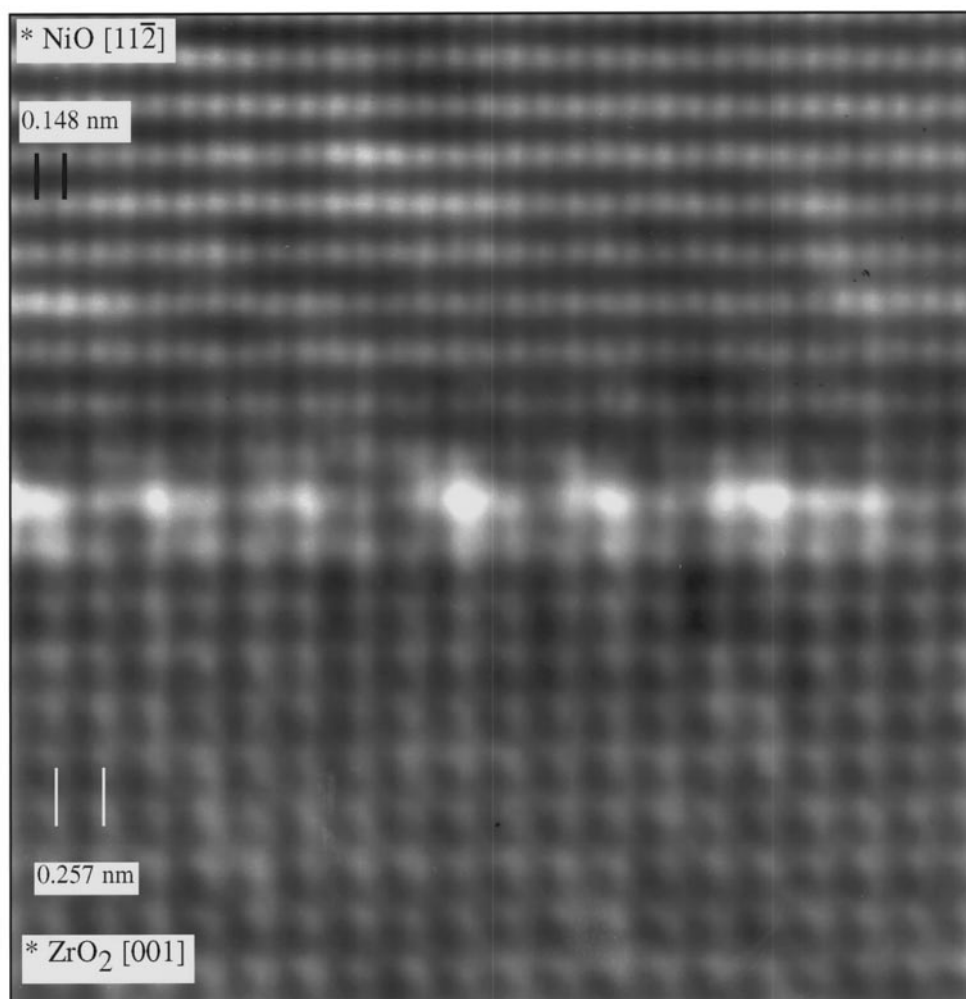


Fig. 9. HREM image of NiO–ZrO₂ along OR II reveals atomic relaxation in the NiO within 0.5 nm of the interface.

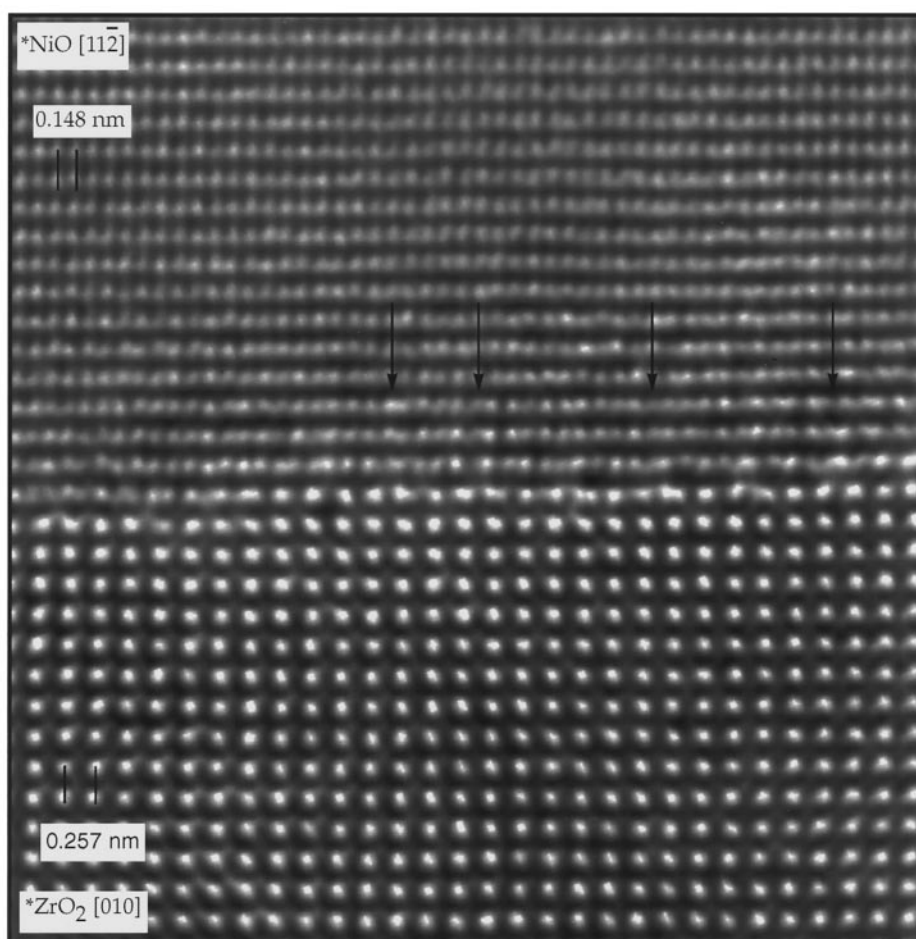


Fig. 10. NiO–ZrO₂ interface imaged along OR II imaged on the Stuttgart JEOL JEM-ARM1250 shows atomic relaxations in the NiO near the interface. Although distinct dislocation cores cannot be resolved some NiO (220) planes do disappear near the boundary; these are identified by arrows.

dislocations are identified with arrows in Fig. 10. The HREM results from OR II indicate that the interface is fully relaxed with localized accommodation of misfit occurring primarily in NiO. No long-range periodicity is observed, which is expected since the two lattices are incommensurate as viewed from this projection. Although a continuity of lattice planes is not maintained across the interface, the local atomic relaxations indicate that there is interaction between the phases across the boundary and, in that sense, the interface cannot be considered incoherent.

Although the HREM studies reveal the presence of NiO relaxation, the extent of the relaxation cannot be quantified directly from the images; quantitative HREM analysis would require an iterative multislice simulation study using a variety of relaxed models. Z-contrast imaging coupled with maximum entropy calculations, on the other hand, allows us to directly measure cation positions and interplanar spacings. Figure 11 is a Z-contrast image along OR II which reveals displacement of

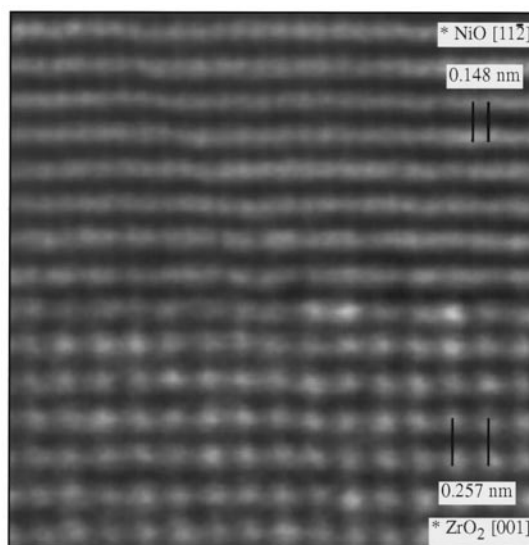


Fig. 11. Z-contrast image along OR II reveals displacement of the Ni atoms from their bulk lattice sites near the interface.

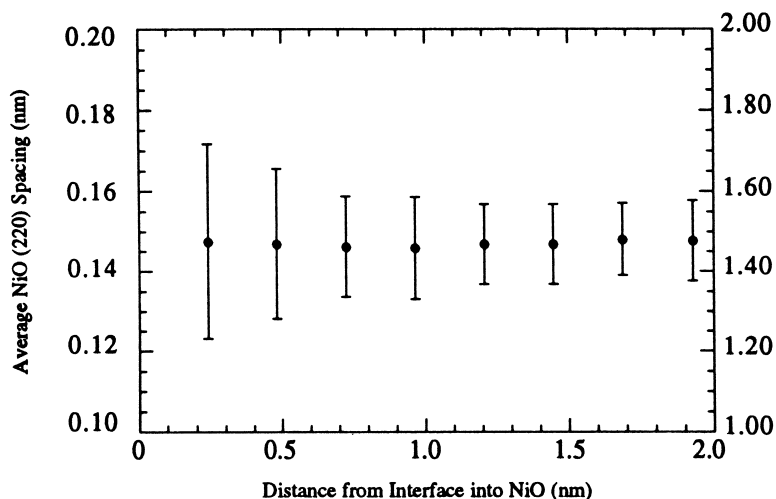


Fig. 12. Measurements taken from maximum entropy calculations show that the average lattice spacing of the NiO (220) remains constant near the interface, but the standard deviation increases by a factor of two due to local atomic relaxations.

the Ni atoms from their bulk lattice sites near the interface, consistent with HREM studies. Measurements taken from maximum entropy calculations are presented in Fig. 12. Note that although the mean NiO (220) spacing does not vary significantly, the standard deviation of the spacing increases by a factor of two at the interface as compared to the bulk. The standard deviation in the bulk (0.01 nm) is a consequence of the pixel resolution of the image, in this case 64.4 pixels/nm, which limits the measurement accuracy. The excess in the standard deviation at the interface arises from relaxations in the NiO along $[\bar{1}10]$, yielding a root mean square relaxation of 0.02 nm in the Ni plane adjacent to the interface.

The strain in the NiO lattice leads to coordination changes which should be reflected in the EELS oxygen K near-edge fine structure. To check for consistency, profiles of the O K edge were taken from the interface towards the bulk NiO in steps of interplanar spacing. A chi-squared (χ^2) fit to a bulk spectrum was calculated using the noise before the edge onset as a measure of the standard deviation. The results of the χ^2 fitting reveal perturbations of the fine structure out to the third oxygen plane from the interface (see Fig. 13). Rez *et al.* [30], using XANES multiple scattering calculations, showed that the O K near-edge fine structure in NiO is dominated by scattering within the first oxygen shell and the first two Ni shells. The spatial extent of the fine structure perturbation in this experiment, therefore, correlates well with the spatial extent of the distorted NiO lattice.

Several other studies also indicate that ionic interfaces tend to relax to low-energy configurations through local atomic relaxations. Partially coherent interfaces containing coherency and anticoherency dislocations are found at TiO₂-sapphire [1], Fe₂O₃-

Al₂O₃ [29] Mo₃Si₅-MoSi₂ [10] and MgO-Al₂O₃ [6]. These results and the evidence for local relaxation at the NiO-ZrO₂ interfaces suggest that ionic heterophase systems do tend to relax to configurations which promote localized bonding across the interface. Detailed investigations of dislocation core structures, however, are lacking.

3.5. In-plane rigid body translation (RBT)

In-plane RBTs constitute two microscopic degrees of freedom of a crystalline interface and are important relaxations mechanisms by which the interface can achieve a low-energy configuration.

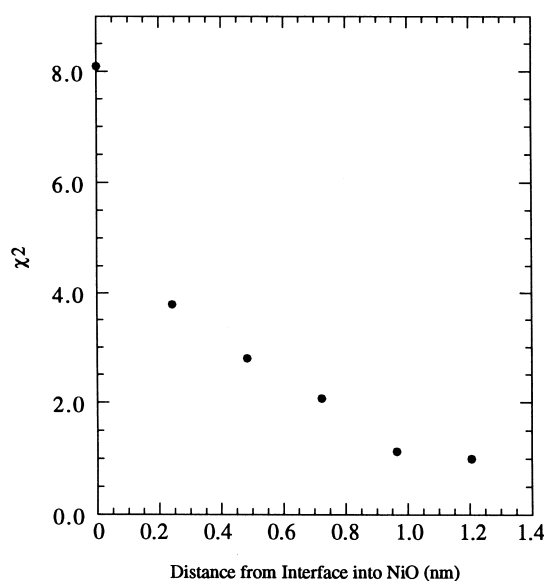


Fig. 13. Chi-squared fit of O K-edge spectra to a bulk NiO spectrum as a function of distance from the interface. The fine structure is perturbed up to about 0.7 nm into the NiO due to distortions in the lattice.

For grain boundaries, the traditional definition of an in-plane RBT is any RBT which destroys the coincident site lattice (CSL). A more rigorous definition which holds for both homo- and heterophase boundaries defines an in-plane RBT as a relative translation of the two crystals parallel to the interface which lowers the bicrystal symmetry below that of the unrelaxed holosymmetric bicrystal [31]. The unrelaxed holosymmetric bicrystal maintains the maximum-possible bicrystal symmetry.

For the case of the NiO–ZrO₂ bicrystal, the maximum-possible projected point symmetry and holosymmetric symmetry are illustrated in Fig. 14. Convergent beam electron diffraction (CBED) studies of plan-view specimens (OR III), show that the NiO–ZrO₂ bicrystal does indeed display the maximum possible $2mm$ projected diffraction symmetry and m whole pattern symmetry [32]. Since the bicrystal maintains the maximum possible symmetry, it is said to have zero in-plane RBT. The RBT, however, does not provide a unique solution for the interface structure. Pond showed that a multiplicity of boundary structures (neglecting local atomic relaxations) exist for a given translational symmetry of a bicrystal [33], and as will become evident in the following discussion, the maximum possible boundary structures for the NiO–ZrO₂ system is six.

The one-dimensional periodicity of the NiO–ZrO₂ bicrystal limits the relevance of in-plane RBT to only one direction, namely $[11\bar{2}]_{\text{NiO}} \parallel [001]_{\text{ZrO}_2}$. Along this direction, the terminating NiO plane at the interface may reside in six specific positions relative to the ZrO₂ lattice while maintaining the maximum bicrystal symmetry. The six resulting models, projected along OR I, are presented in Fig. 15. Each model corresponds to a different plane in the FCC stacking sequence terminating at the interface with the Ni sites situated either over

Zr or O sites in the ZrO₂ lattice. Although each model has identical bicrystal symmetry, the atomic configurations for each are distinct with perhaps different interfacial energies, and it is therefore important to distinguish the prevailing configuration. The boundary plane location is therefore an independent degree of freedom; this is true for any bicrystal that does not have a monoatomic basis [28].

The most direct method for determining the relative translations of the NiO and ZrO₂ is analyzing Z-contrast images taken along OR I. The correct model (model e in Fig. 15) is the one superimposed on the Z-contrast image in Fig. 7. (The translational model identified by Z-contrast was also the model used for HREM multislice simulations as presented in Section 3.3.) Note that this model is characterized by a projected common oxygen plane which is continuous with the projected oxygen planes in both the NiO and the ZrO₂. The continuity of the projected oxygen sublattice across the interface suggests that the anion sublattice (and not the cation sublattice) plays a dominant role in determining the low-energy interface structure.

3.6. Interface model

By using HREM, Z-contrast imaging and EELS as complementary techniques, we now have a detailed understanding of the three-dimensional atomic structure of the NiO–ZrO₂ interface. The NiO–ZrO₂ bicrystal has an atomically sharp transition between the two phases at the interface with a common oxygen plane facilitating the chemical transition. Although the structural width of the boundary also appears atomically sharp along OR I, the orthogonal projection reveals a width on the order of 0.5 nm due to local atomic relaxations. This structural width is asymmetric about the interface since NiO incurs most of the relaxation. The

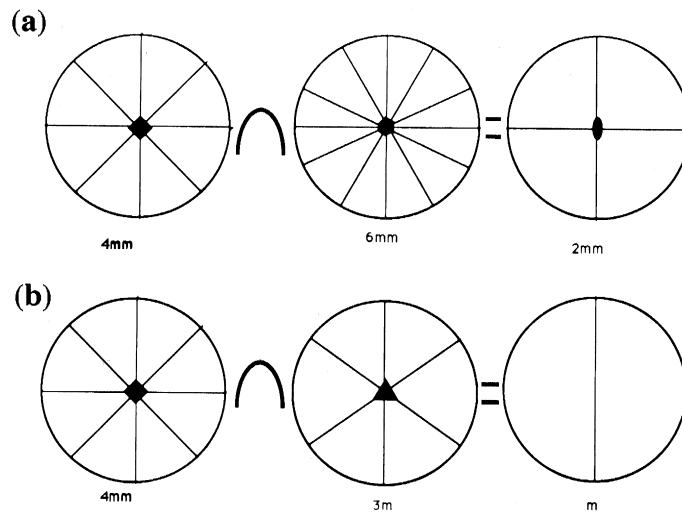


Fig. 14. Schematic representation of the maximum-possible bicrystal symmetry for a NiO–ZrO₂ bicrystal, including (a) projected point symmetry and (b) three-dimensional symmetry.

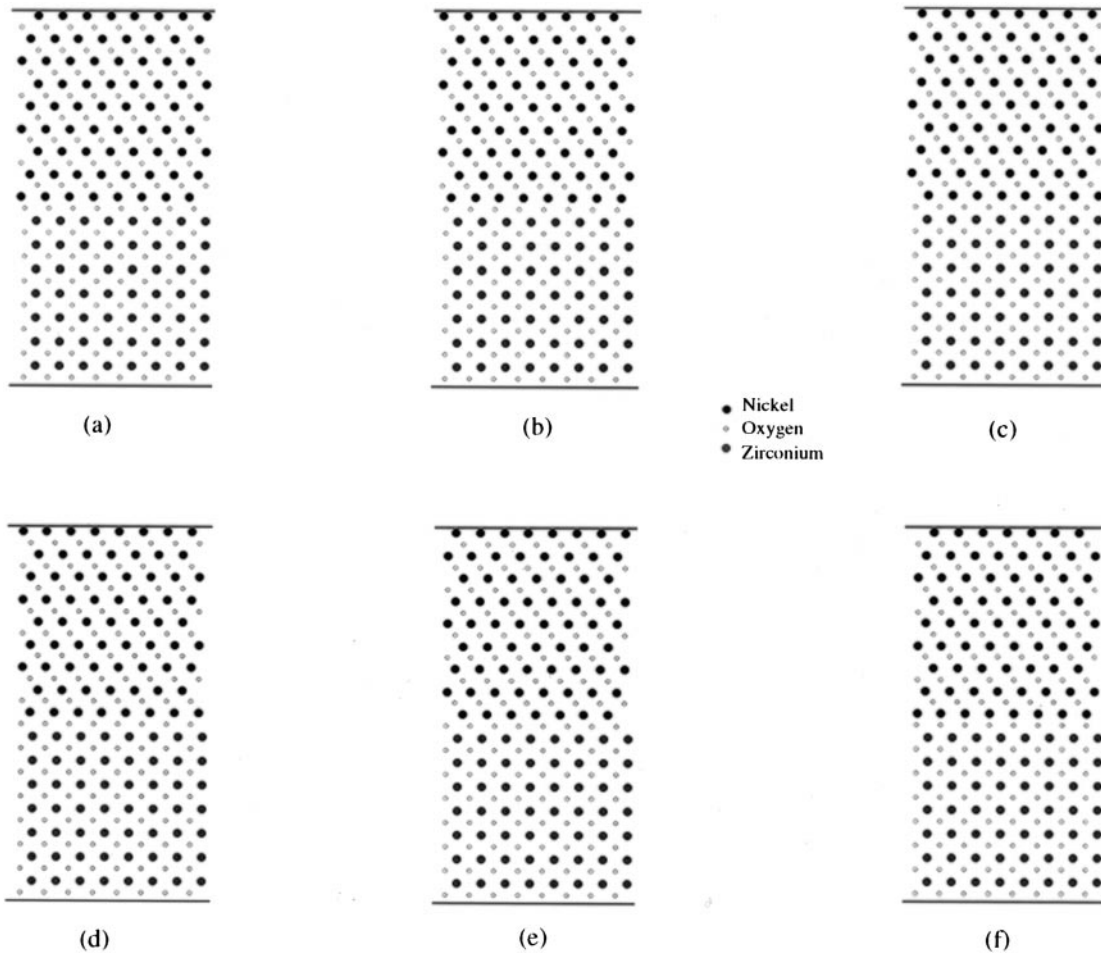


Fig. 15. Six NiO–ZrO₂ interfacial models which maintain the maximum bicrystal symmetry.

interface structure implies that the atoms in the NiO within about 0.5 nm are relaxing along $[\bar{1}10]$ to positions away from the NiO lattice to positions more consistent with the ZrO₂ lattice. The transition in symmetry and oxygen coordination thus appears to be accommodated by distortions of the NiO lattice near the interface.

From these experimental findings, an atomic model for the NiO–ZrO₂ interface was derived. To develop a model for the local atomic relaxations, an algorithm was written which displaces the NiO lattice geometrically along $[\bar{1}10]$ towards positions corresponding to the ZrO₂ lattice. Figure 16 is a model of the interface in plan-view showing the unrelaxed Ni positions and relaxed Ni positions which have been displaced along $[\bar{1}10]$ towards the Zr sublattice. The maximum magnitude of the relaxation was constrained by the experimentally determined strain (Section 3.4). The algorithm decays the displacements linearly to zero over five planes (3 Ni and 2 O) in the NiO. The resulting three-dimensional structure viewed along two orthogonal directions (OR I and OR II) is presented in Fig. 17. Note that atoms in each NiO (220) plane move collectively and that the planes bend towards each other, simi-

lar to experimental images. Although the projected lattice strains are as high as $\pm 16\%$, this is a plausible relaxation mechanism since the interatomic distances change by a maximum of only $\pm 4.6\%$.

The interface structure has several implications for bonding at the interface. Figure 18 is a SEM image of a crack (initiated by a Vickers indentation) which has propagated through the NiO–ZrO₂ microstructure. The crack does not deflect along the interface, but rather propagates in the ZrO₂. This fracture behavior in which cracks do not tend to debond the interface is quite common in most oxide DSE systems [34]. This study on the structure of NiO–ZrO₂ DSE interface, although it does not rationalize the fracture behavior, sheds light on the mechanical robustness of such *in-situ* composite interfaces. First of all, the integrity of the interface (no voids, second phases, etc.) allows the two phases to be in intimate contact at the boundary and does not provide any macroscopic stress concentrators. Because the two phases share a common oxygen plane at the boundary, the electrostatic attraction between the anion and cation planes serves as a bonding mechanism in this ionic system. Just as single crystals do not tend to cleave along

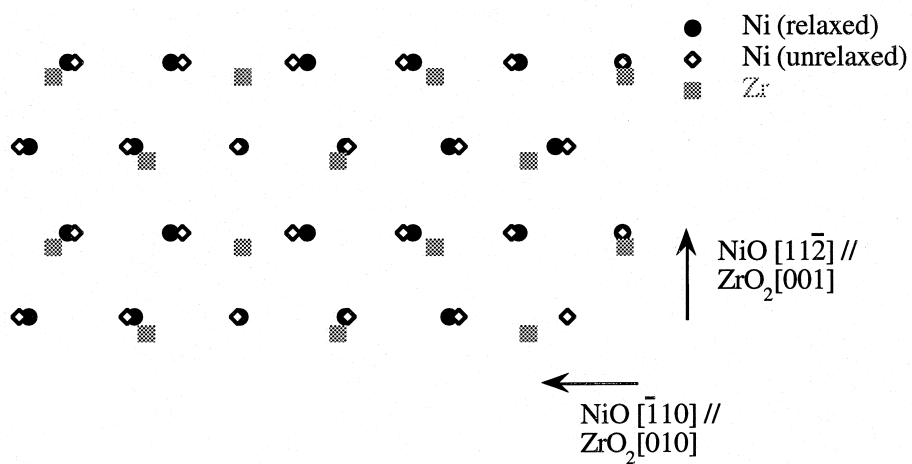


Fig. 16. Plan view of the NiO-ZrO₂ interface showing the displacement of Ni sites along [$\bar{1}10$] towards the Zr sublattice.

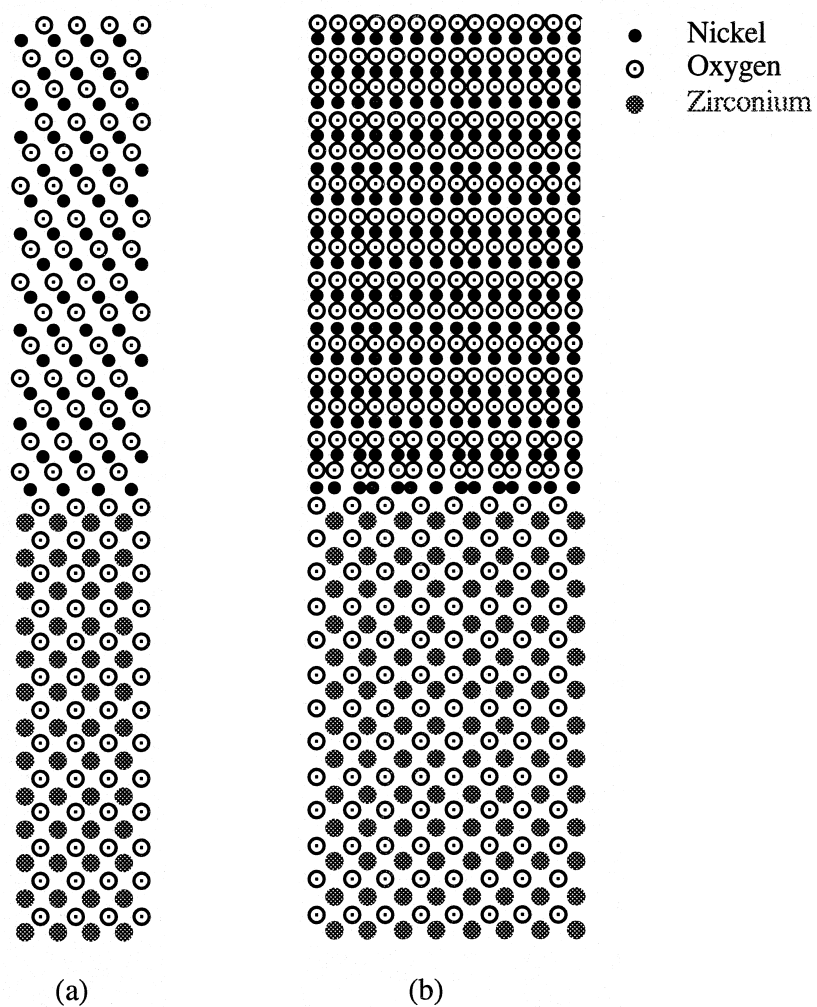


Fig. 17. Three-dimensional model of the relaxed NiO-ZrO₂ interface projected along (a) OR I and (b) OR II.

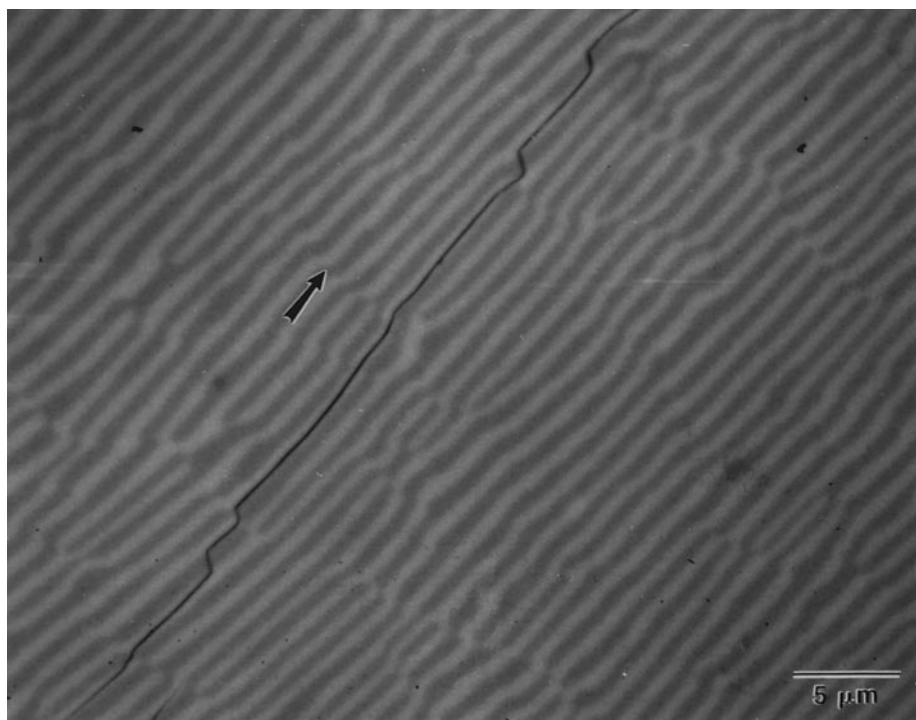


Fig. 18. SEM backscattered image of an indentation-induced crack propagating through the NiO (dark phase) and ZrO₂ (light phase) microstructure. The arrow indicates the direction of crack propagation. The crack interacts with the NiO–ZrO₂ DSE microstructure, but does not tend to debond the interface.

directions which will expose two polar surfaces, this interface also should not cleave easily. In addition, the evidence for local relaxation of the interfaces indicates that the interface is in a low-energy configuration with a maximum cohesive energy.

4. SUMMARY AND CONCLUSIONS

Summarizing the experimental findings of the NiO–ZrO₂ interface structure:

(1) We find considerable evidence indicating that the NiO–ZrO₂ boundaries are low-energy interfaces: (a) the interfaces are free to form low-energy configurations during the solidification process since the only constraints on the system are gravity and the temperature gradient [10], (b) macroscopically curved boundaries are composed of steps and ledges with the step ledges maintaining the predominant orientation relationship [10], (c) the lattice bending in NiO along $[\bar{1}10]$ indicates that the boundary has relaxed to a low-energy configuration.

(2) Chemically, the NiO–ZrO₂ interface is atomically abrupt.

(3) The orientation relationship between NiO and ZrO₂ results in a layered structure of anions and cations across the boundary. The two phases share a common oxygen plane at the interface giving rise to electrostatic bonding across the boundary.

(4) Local atomic relaxations are present in the NiO near the interface indicating that the interface is in a relaxed, low energy configuration. The local

atomic relaxations, however, are confined to one dimension, namely NiO $[\bar{1}10]$.

(5) The symmetry of the bicrystal, as determined by CBED, restricts the in-plane RBT to six configurations. The prevailing configuration as determined by both Z-contrast and HREM maintains a continuity of the oxygen sublattice across the boundary as projected along OR I.

Although this study has provided insight into the structure of ionic heterophase interfaces, it serves only as a starting point to the ultimate goal of establishing predictive structure–property relationships for interface-influenced or controlled systems. Bimaterials are typically studied on several length scales, from the macroscopic and continuum levels down to the atomic and electronic levels; each length scale is distinguished by what is considered collectively and distinctly in the analysis [35]. Although much progress has been made in understanding composite behavior at each of these length scales (in this study the atomic scale), there is a definite lack of continuity between the different levels; connections between the length scales are not thoroughly understood. To study the role of the interface in bimaterial systems continuously through all of the length scales, it is prudent to examine model systems which facilitate analysis from the atomic to macroscopic level. The NiO–ZrO₂ eutectics studied here provide an excellent opportunity to study fracture behavior in brittle composites,

because the microstructure facilitates investigation on all length scales. We intend to build upon the atomic-level studies presented in this paper, by investigating the fracture behavior with respect to the crystallography, microstructure and residual stresses. By working our way up in length-scale magnitude in a continuous manner, we will ultimately be able to understand the fracture behavior of the NiO–ZrO₂ DSE composite and be able to predict the behavior of similar materials.

Acknowledgements—The authors would like to thank Alex Revcolevschi of the Université de Paris-Sud for supplying the DSE specimens. We would also like to extend sincere thanks to Manfred Rühle and the Max Planck Institute, Stuttgart for facilitating the ARM sessions and to Thomas Gemming for his assistance in operating the ARM. This material is based upon work supported under a National Science Foundation Graduate Research Fellowship (for E.C.D.) and NFS-DMR grant no. 95284888. This research was also supported by U.S. Department of Energy contract No. DE-AC05-96OR22464, as part of the ORNL HTML Fellowship Program with Lockheed Martin Energy Research Corp. (for E.C.D.) and ORNL Postdoctoral Program administered by Oak Ridge Institute for Science Education (for P.N.).

REFERENCES

- Merkle, K. L., Buckett, M. I. and Gao, Y., *Acta metall. mater.*, 1992, **40**, S249.
- Muschik, T. and Rühle, M., *Philos. Mag. A*, 1992, **65**, 363.
- Necker, G. and Mader, W., *Philos. Mag. Lett.*, 1988, **58**, 205.
- Chisholm, M. F., Pennycook, S. J., Jevasinski, R. and Mantl, S., *Appl. Phys. Lett.*, 1994, **64**, 2409.
- Chen, F. R., Chiou, S. K., Chang, L. and Hong, C. S., *Ultramicroscopy*, 1994, **54**, 179.
- Li, D. X., Pirouz, P. and Heuer, A. H., *Philos. Mag. A*, 1992, **65**(2), 403.
- Carter, C. B. and Schmalzried, H., *Philos. Mag. A*, 1985, **65**(2), 207.
- Heuer, A. H., Lanteri, V. and Chaim, R., *Ultramicroscopy*, 1987, **22**, 27.
- McKernan, S. and Carter, C. B., *Ultramicroscopy*, 1989, **30**, 256.
- Xiao, S. Q., Maloy, S. A., Heuer, A. H. and Dahmen, U., *Philos. Mag. A*, 1995, **65**(4), 997.
- Dravid, V. P., Lyman, C. E., Notis, M. R. and Revcolevschi, A., *Ultramicroscopy*, 1989, **29**, 60.
- Dahmen, U., *MSA Bull.*, 1994, **24**(1), 341.
- Browning, N. D., Chisholm, M. F. and Pennycook, S. J., *Nature*, 1993, **333**, 143.
- Batson, P. E., *Nature*, 1993, **366**, 727.
- Dhaleene, G. and Revcolevschi, A., *J. Cryst. Growth*, 1984, **69**, 616.
- Phillipp, F., Hörschen, R., Osake, M., Möbus, G. and Rühle, M., *Ultramicroscopy*, 1994, **56**, 1.
- Jesson, D. E. and Pennycook, S. J., *Proc. R. Soc. Lond. A*, 1993, **441**, 261.
- Jesson, D. E. and Pennycook, S. J., *Proc. R. Soc. Lond. A*, 1995, **449**, 273.
- Nellist, P. D., Pennycook, S. J., *Scanning Microsc.*, in press.
- Gull, S. F. and Skilling, J., *IEE Proc.*, 1984, **131F**, 646.
- Brydson, R., Sauer, H., Engel, W., in *Transmission Electron Energy Loss Spectrometry in Materials Science*, ed. M. M. Disko, C. C. Ahn, B. Fultz. The Minerals, Metals, and Materials Society, 1992.
- Edgerton, R. F., *Electron Energy Loss Spectroscopy in the Electron Microscope*. Plenum Press, New York, 1986.
- Holbrook, O. F. and Bird, D. M., *Inst. Phys. Conf. Ser.*, 1995, **147**, 175.
- Holbrook, O. F., Bird, D. M., in *Proceeding Microscopy and Microanalysis*, Vol. 278. Jones and Begell Publishing, New York, 1995.
- Revcolevschi, A., Dhaleene, G. and d'Yvoire, F., *J. Phys.*, 1985, **46**, C4.
- Fragneau, M., Revcholevschi, A., *J. Am. Ceram. Soc.*, 1982, **65**, C-102.
- Fragneau, M., Revcholevschi, A., *J. Am. Cer. Soc.*, 1983, **66**, C-162.
- Mazerolles, L., Michel, D., Cornier M., Portier, R. *Advances in Ceramics*, Vol. 24, *Science and Technology of Zirconia III*. The American Ceramic Society, Inc., 1988, p. 471.
- Tietz, L. A. and Carter, C. B., *Philos. Mag. A*, 1993, **67**(3), 699.
- Rez, P., Bruley, J., Brohan, P., Payne, M. and Garvie, L. A. J., *Ultramicroscopy*, 1995, **59**, 159.
- Sutton, A. P., Balluffi, R. W., *Interfaces in Crystalline Materials*. Oxford Science Publications, Clarendon Press, Oxford, 1995.
- Dravid, V. P., Notis, M. R., Lyman, C. E., Revcolevschi A., *Mat. Res. Soc. Symp. Proc.*, Vol. 159. Materials Research Society, 1990, p. 95.
- Pond, R. C., Bacon, D. J., Serra, A. and Sutton, A. P., *Metall. Trans. A*, 1991, **22A**, 1185.
- Hulse, C. O., Batt, J. A., Final Technical Report, UARL-N910803-10, NTIS AD-781995/6GA, 1974.
- King, W. E., Campbell, G., Gonis, T., Hanshall, G., Lesuer, D., Zywicz, E. and Foiles, S., *Mater. Sci. Eng. A*, 1995, **191**, 1.